Original Research Article

Dynamic three-dimensional coculture model: The future of tissue engineering applied to the peripheral nervous system

Journal of Tissue Engineering
Volume 15: 1–18

DOI: 10.1177/20417314241265916
journals.sagepub.com/home/tej
Sage

William Choinière[1], Ève Petit[1], Vincent Monfette[1], Samuel Pelletier[2], Catherine Godbout-Lavoie[1] and Marc-Antoine Lauzon[1,3,4]

Abstract

Traumatic injuries to the peripheral nervous system (PNI) can lead to severe consequences such as paralysis. Unfortunately, current treatments rarely allow for satisfactory functional recovery. The high healthcare costs associated with PNS injuries, worker disability, and low patient satisfaction press for alternative solutions that surpass current standards. For the treatment of injuries with a deficit of less than 30 mm to bridge, the use of synthetic nerve conduits (NGC) is favored. However, to develop such promising therapeutic strategies, *in vitro* models that more faithfully mimic nerve physiology are needed. The absence of a clinically scaled model with essential elements such as a three-dimension environment and dynamic coculture has hindered progress in this field. The presented research focuses on the development of an *in vitro* coculture model of the peripheral nervous system (PNS) involving the use of functional biomaterial which microstructure replicates nerve topography. Initially, the behavior of neuron-derived cell lines (N) and Schwann cells (SC) in contact with a short section of biomaterial (5 mm) was studied. Subsequent investigations, using fluorescent markers and survival assays, demonstrated the synergistic effects of coculture. These optimized parameters were then applied to longer biomaterials (30 mm), equivalent to clinically used NGC. The results obtained demonstrated the possibility of maintaining an extended coculture of SC and N over a 7-day period on a clinically scaled biomaterial, observing some functionality. In the long term, the knowledge gained from this work will contribute to a better understanding of the PNS regeneration process and promote the development of future therapeutic approaches while reducing reliance on animal experimentation. This model can be used for drug screening and adapted for personalized medicine trials. Ultimately, this work fills a critical gap in current research, providing a transformative approach to study and advance treatments for PNS injuries.

Keywords

Peripheral nerve injuries, perfusion bioreactor, biomaterials, neuronal cells, collagen, chitosan

Date received: 3 April 2024; accepted: 18 June 2024

Introduction

Present-day medicine offers the potential for miraculous advancements to elevate the quality of life for individuals coping with a range of injuries and traumas. In some extreme cases, such as nerve severance, patients may need surgical interventions to hope for a satisfactory level of autonomy and functionality. Injuries to the peripheral nervous system (PNI) constitute a major clinical and economic problem worldwide, affecting all sectors of the population.[1–5] Indeed, patients suffering from PNI experience a significant decrease in their quality of life.[6,7] PNI

[1]Department of Chemical Engineering and Biotechnological Engineering, Université de Sherbrooke, Sherbrooke, QC, Canada
[2]Department of Electrical and Informatics Engineering, Université de Sherbrooke, Sherbrooke, QC, Canada
[3]Research Center on Aging, CIUSS de l'ESTRIE-CHUS, Sherbrooke, QC, Canada
[4]The Quebec Network for Research on Protein Function, Engineering, and Applications, Montréal, QC, Canada

Corresponding author:
Marc-Antoine Lauzon, Department of Chemical Engineering and Biotechnological Engineering, Université de Sherbrooke, 2500 Blvd Université, Sherbrooke, QC J1K2R1, Canada.
Email: marc-antoine.lauzon@usherbrooke.ca

cause multiple symptoms such as untreatable neuropathic pain, muscle weakness and atrophy,[8] loss of sensory or motor functions, or even complete paralysis of the affected limb.[9] These injuries are widespread, as it is estimated that PNI currently affect more than 20 million people in the USA alone,[10] representing 2% to 3% of all traumas affecting extremities (e.g. arms, legs).[11] Moreover, it is worth mentioning that the majority of these PNI require surgical nerve reconstruction. According to a meta-analysis,[12] only 51.6% of individuals affected by these injuries satisfactorily recover their motor functions, while only 42.6% achieve satisfactory sensory recovery.

Microsurgery is essential for repairing cross-sectional nerve injuries, where end-to-end nerve connections must be made without tension to avoid ischemia; otherwise, nerve grafts are needed to bridge the gaps.[13–17] Currently, various types of nerve guidance conduits (NGCs) smaller than 30 mm in length and 5 mm in diameter are clinically used to repair nerve losses. Some of them have even shown better results than autografts.[18,19] However, none has proven to yield equivalent or superior results to autografts for segments exceeding 30 mm, thus autografts are still recognized as the gold standard in clinical practice for this type of larger-scale lesion.[20] Nevertheless, several limitations hinder the full realization of the potential of new therapeutic strategies. Among these limitations is the lack of reliable models to test these emerging technologies and knowledge regarding nerve regeneration phenomena remains insufficient in certain circumstances.

The first generation of three-dimension *in vitro* models for PNI often confined themselves to using a single cell type, rendering them obsolete due to their lack of tissue realism in representing the *in vivo* environment. This limitation results in deficiencies in functionality and cellular representation when compared to coculture models.[21,22] While regenerative processes require a close collaboration among several types of cells such as macrophages and satellite glial cells to promote axonal growth, SCs cells are the main actors involved in nerve homeostasis and regeneration.[15,23–25] Among other functions, SCs create a favorable environment for the maintenance and protection of neurons by expressing various elements such as constituents of the extracellular matrix, adhesion molecules, integrins, and growth factors such as neurotrophins.[26–28] They also play a central role during axonal regeneration by recruiting macrophages, clearing cellular debris, secreting growth factors and providing axonal guidance through the formation of bands of Büngner.[29] Several studies have explored the advantages of coculture between SCs and neurons in axonal regeneration.[30–34] These studies have suggested that the presence of SCs in the coculture is crucial for the survival, axonal growth, and myelination of motor neurons. Coculture, therefore, emerges as a critical feature in the development of a robust *in vitro* model.

Maximizing the in vivo characteristics of a nerve repair model is also crucial to replicate the organized and aligned microstructural physiology (anisotropy) of the peripheral nervous system (PNS), a feature seldom found in the majority of current cellular models. Engineered three-dimension structures such as NGC can promote the infiltration, growth and alignment of cells, facilitating gas and nutrient exchanges.[35] While only a limited number of studies have integrated coculture with biomaterials,[36–41] they have demonstrated that this combination enables the exploration of cellular interactions and the impact of implant and material characteristics on neural regeneration in a three-dimension mimetic PNS environment.

Unfortunately, most three-dimension models found in the scientific literature use static culture conditions to study regenerative phenomena, limiting the development of therapeutic strategies due to a gap in mass transfer within the biomaterial.[36] In addition to contradicting the physiology of the PNS, which involves constant nutrient exchange due to the presence of numerous blood vessels, these static models have been shown to limit nutrient distribution, oxygen diffusion, and cellular waste removal within the material. This negatively impacts the survival, proliferation, colonization, and differentiation of the key cellular actors involved in the regeneration process,[42] along with the dimensions and scale of *in vitro* models.[43] While dynamic coculture models provide the capacity to maintain decent viability for an extended period with the possibility of homogeneously distributing nutrients, most of these systems are still operated at the microfluidic scale,[44–49] which are less expensive and easier to control. However, these models rarely exceed 10 mm,[50] a dimension that is not representative of human PNI, which can extend over several centimeters. This limitation restricts their translatability to human scenarios. To overcome those limitations and recapitulate more precisely the physiological environment of human size PNS, the new generation of *in vitro* coculture models should therefore combine key characteristics such as anisotropic functional biomaterials extending several centimeters and dynamic culture conditions.

Consequently, this study reports the development of a three-dimensional dynamic coculture model with a clinically relevant size to study Schwann and neuronal cells behaviors, which is unprecedented in the field. The integration of these distinctive attributes renders this model unparalleled within its domain, providing functionalities that more accurately mimic *in vivo* environments. Cells were cultured in contact with collagen/chitosan composite scaffolds several centimeters in length, featuring longitudinally aligned micro-channels. These scaffolds were continuously perfused, aiming to support long-term coculture and enhance colonization, viability, and functionality. Such a model will facilitate the optimization of the new generation of NGCs and accelerate nerve regeneration by

enabling pre-clinical trials of promising therapeutic strategies through the presentation of a three-dimensional coculture model of clinical size under dynamic conditions.

Materials and methods

Materials

Purified type I collagen from bovine Achilles tendon was purchased from MyBioSource (San Diego, CA, USA). Medium molecular weight chitosan (75%–85% deacetylated), mouse laminins (L2020) as well as crosslinking agents, EDC (N-(3-dimethylaminopropyl)- N'- ethylcarbodiimide), NHS (N-hydroxysuccinimide), TPP (sodium triphosphate pentabasic) and poly-L-lysine hydrobromide (PLL), Triton™ X-100, Normal Goat Serum (NGS) and supplement for NG108-15 medium such as, hypoxanthine, aminopterin, thymidine and sodium bicarbonate were purchased from Millipore-Sigma (Oakville, ON, CA). Polydimethylsiloxane (PDMS) SYLGUARD™ 184 Silicone Elastomer Kit was purchased from Ellsworth Adhesives Canada (Stoney Creek, ON, CA). Schwann cells (S16 line, CRL-2941™) and Neuron somatic cell hybrids from mouse neuroblastoma (NG108-15 line, HB-12317™) were obtained from Cedar Lane Labs (Burlington, ON, CA). Fetal Bovine Serum (FBS) was purchased from Wisent Bioproducts (St-Jean-Baptiste, QC, CA). Dulbecco's modified Eagle's medium (DMEM, high glucose, GlutaMAX supplement, with and without pyruvate), penicillin-streptomycin (Pen Strep), Peprotech β-Nerve Growth Factor (β-NGF) (Catalog #: 450-01), Hoechst 33342 and Live/Dead™ Viability/Cytotoxicity Kit (Invitrogen) reagents, CellTracker™ Blue CMAC Dye (Catalog number: C2110) and CellTracker™ Deep Red Dye (Catalog number: C34565) (Invitrogen) were purchased from Life Technologies (Burlington, ON, CA). Primary and secondary antibodies (Cell Signalling Technology inc): S100β (E7C3A) Rabbit mAb 90393 (dilution 1/200), β3-Tubulin (TU-20) Mouse mAb #4466, Myelin Protein Zero antibody (Catalog # : 57518S), Anti-rabbit IgG (H+L), F(ab')2 Fragment (Alexa Fluor® 488 Conjugate Green) 4412 and Anti-mouse IgG (H+L), F(ab')2 Fragment (Alexa Fluor® 647 Conjugate) #4410 were purchased from New England Biolabs Ltd (Whitby, ON, CA).

Scaffold preparation

Biopolymers and scaffold preparation were produced as we have previously reported.[51] Collagen-chitosan composite scaffolds were produced using an 80:20 weight ratio as it demonstrated to be the best biomaterial composition in terms of mechanical properties and cytocompatibility. Briefly, the process started with creating a 1% (w/w) collagen/chitosan 80/20 (weight ratio) solution in 3.8% (w/v) acetic acid. The solution needed to be well homogenized in an ice bath using an overhead homogenizer (LabGEN 125, Cole-Parmer Canada Inc.). This solution was then cleared of air bubbles by centrifugation and degassing in a vacuum chamber. Afterward, the scaffolds were molded using a unidirectional freeze-casting method as previously reported.[51] The frozen structures were then subjected to freeze-drying to remove water and create the characteristic micro-channel structure aligned in the direction of the thermal gradient. The resulting anisotropic scaffolds were then chemically crosslinked with EDC (33 mM)-NHS (6 mM) chemistry to increase their strength and resistance to degradation. The scaffolds were then sequentially washed in ethanol solutions and deionized water, flash-frozen in liquid nitrogen and freeze-dryed for long-time storage. The scaffolds were then stored in a desiccator until they were needed for experimentations.

Prior to being used in experiments, scaffolds were sterilized by soaking in 70% (v/v) ethanol overnight. Scaffolds were then washed three times using PBS 1× before the samples underwent laminin adsorption by incubation at 37°C (Forma Series II, ThermoFisher) for 2 h in a 15 µg/mL laminin-PBS 1× solution and then washed again three times to make fully prepared scaffolds.

Scanning electron microscopy

To validate the synthesis method and assess the scaffold pore and channel structure before experimentations, images of transversal and longitudinal cuts from crosslinked scaffolds were obtained using a benchtop scanning electron microscope (SEM) (Phenom XL, ThermoFisher) as previously described in Monfette et al.[51] Briefly, samples taken at the top, bottom and middle of each scaffold were prepared by doing transversal and longitudinal cut with a surgical scalpel blade. Cut samples were then fixed onto metal stubs with conductive carbon tape. Observations were conducted in normal mode under 10 kV acceleration and 0.1 to 10 Pa.

Cells culture

Schwann cells (S16 line from sciatic nerve of rats, CRL-2941™) were cultivated on cell culture-treated flasks coated with 15 µg/mL PLL in high glucose DMEM containing glutamine and pyruvate, and supplemented with 10% (v/v) FBS, 1% (v/v) penicillin-streptomycin. Cells were incubated at 37°C with 5% CO_2 in a humidified atmosphere (Forma Series II, ThermoFisher) and passaged by trypsinization every 2–3 days. Cells were used under 15 passages.

Neuron somatic cell hybrids from mouse neuroblastoma (NG105-15 line, HB-12317™) were cultivated on cell culture-treated flasks in DMEM without pyruvate, supplemented with 0.1 mM hypoxanthine (final conc.), 400 nM aminopterin (final conc.), 0.016 mM thymidine

(final conc.), 10% (v/v) fetal bovine serum, 18 mM sodium bicarbonate and 1% (v/v) penicillin-streptomycin. Cells were incubated at 37°C with 5% CO_2 in a humidified atmosphere (Forma Series II, ThermoFisher) and passaged every 2–3 days by trypsinization (Trypsin–EDTA 0.25%). Cells were used under 15 passages. This cell line has been utilized as a reliable neuronal model in studies such as Daud et al.[41] and Hong et al.[50]

For coculture, Schwann cells and NG108-15 cells were initially co-seeded directly onto samples at varying density ratios, depending on the experiment, in coculture medium. The coculture medium corresponded to a volumetric ratio of 1:4 S16 culture medium: NG108-15 culture medium as previously reported in Hong et al.[50] Cocultures were maintained for 7 days at 37°C with 5% CO_2. The medium was replaced with fresh medium supplemented with 5 ng/mL Nerve Growth Factor (NGF) on day two.

Static condition experiments

For static condition tests, the fully prepared scaffolds were sectioned into 5 mm long segments using a scalpel. A total of 5×10^4 to 6×10^4 cells were added at one extremity of each scaffold segment. Different cell ratios (NG108-15: S16) were tested: 1:100, 1:50, 1:10, 1:3, 1:2, and 1:1. The periods prior to introducing the NG108-15 were evaluated at both $t=0$ h and $t=24$ h following S16 cell seeding. Cell seeded scaffolds were grown in complete growth coculture medium supplemented with 10% (v/v) FBS, for 24 h. After this period, the medium was exchanged for the controls (monoculture of NG108-15 and S16) and the coculture with fresh coculture blend medium (describe in previous subsection) without FBS supplemented with 5 ng/mL NGF for an additional 6 days.

Bioreactor design and fabrication

The dynamic culture experiments employed a closed-loop direct perfusion system custom-made by our team (Figure 1(a)). This system, designed to simultaneously operate three independent culture chambers made of optically clear polydimethylsiloxane (PDMS) (Figure 1(b)), incorporates components predominantly built using 3D-printed Onyx™ (Markforged), a thermoplastic composed of nylon and carbon microfibers, along with 3D-printed tough-PLA, and machined Teflon. The bioreactor system was located within a standard cell culture incubator (Forma Series II, ThermoFisher), maintained at 37°C with 5% CO_2. This configuration enables precise temperature control and efficient gas exchange, facilitated by gaz permeable (O_2 and CO_2) platinum-cured silicone tubing. To optimize contact with incubator air and streamline gas exchange, the tubing was intricately wounded around a 3D-printed tower-like component known as the oxygenator. Completely swollen biomaterials were positioned within the culture chambers for perfusion using modified tweezers. Flow control was managed by a micro-peristaltic pump developed by our team as previously reported by El Kheir et al.,[52] which permits accurate and similar flow rate across each culture chamber with values ranging from 0.01 to 1 mL/min (10–1000 µL/min). Based on a literature review of operational flow rates used by bioreactors studying the peripheral nervous system, such as Schmid et al.,[53] we used flow rates of 10, 50, and 200 µL/min. Each bioreactor lines included a 3-way valve with a luer lock adapter that facilitate the seeding of culture chambers by sterile syringes. The bioreactor housed a culture medium bottle fitted with a magnetic stirring system to consistently perfuse fresh medium into the culture chamber over several days. The system, including control of perfusion flow, stirring intensity, and experiment duration, was managed through a custom-made user interface located on a computer.

Due to the material composition, the complete assembly can be easily sterilized prior to each experiment. Sterilization of the metal, Onyx™, and Teflon components was achieved using 70% ethanol. Other components such as the culture chambers, valves, connectors, and the magnetic rod were also sterilized by submersion in 70% (v/v) ethanol for at least 2 h. The culture medium bottle, air filter, specialized lids facilitating tubing ingress and egress, as well as the platinum-treated silicone tubing, were sterilized by autoclaved before use.

To establish the necessary rotor rotation speeds for achieving desired flow rates in the dynamic experiments, a linear calibration process was conducted as we have previously reported by El Kheir et al.[52] Briefly, the solution's density for perfusion bioreactor calibration was identified using the Thermo Library's (Thermodynamics and Phase Equilibrium component),[54] at atmospheric pressure. A polynomial curve was derived from the water density and temperature. Subsequently, water masses were collected from the three tubes at different RPMs (0.1, 0.5, 1, and 2) over a time periods of 20 min. The results in Figure 1(c)) represent three independent experiments for each tube. The flow rate was calculated by dividing the weight of the collected water by the density and the sample time, corrected for the temperature. Ultimately, the mean of the flow rates was computed, and a calibration curve was derived via linear regression.

Dynamic condition experiments

For dynamic condition tests, the fully prepared scaffolds were sectioned into 30 mm long segments using a scalpel. The 30 mm segments were completely swollen in PBS preceding their application, placed into sterile PDMS culture chambers, and then connected to the closed-loop perfusion bioreactor. Sterile ultra pure water was then perfused for 15 min, after which fresh coculture medium was perfused

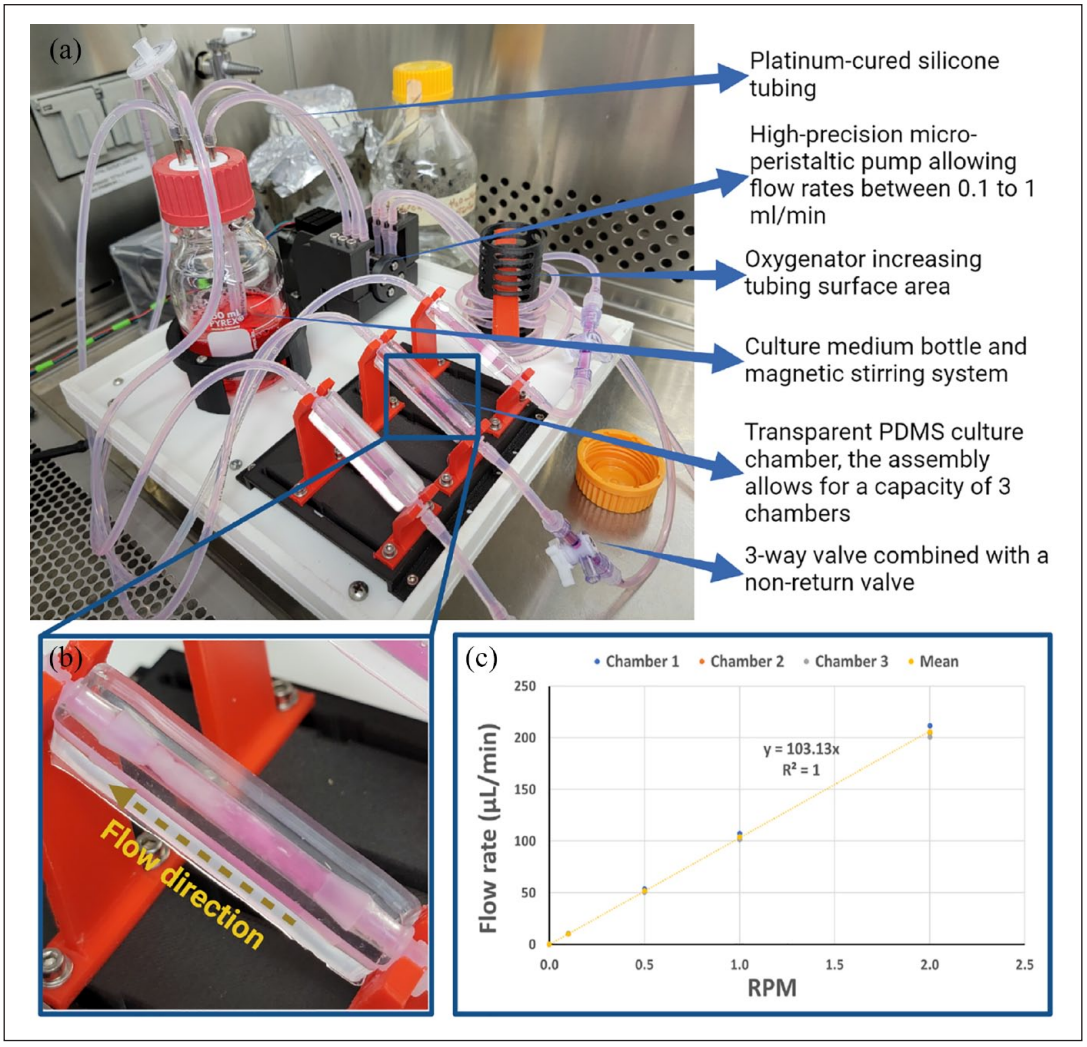

Figure 1. (a) Perfusion bioreactor system, (b) culture chamber with the flow direction, (c) calibration curve of the microperistaltic pump.

for an additional 15 min at 925 µL/min. A three-way valve was opened to enable the injection of a 1:2 [NG108-15: S16] cell suspension, containing a total of 3×10^5 cells in 2 mL, from a syringe attached to the valve. For coculture experiments, a ratio of 1:2 [NG108-15: S16, seeded simultaneously] was used, with both types of cells seeded simultaneously. Seeded scaffolds were then incubated at 37°C in a humidified atmosphere containing 5% CO_2 for 7 days with a perfusion flow of 150 µL/min.

Cell viability and colonization tests

CellTracker™ assays were utilized for the observation of cell colonization ans distribition at the scaffold interface according to the manufacturer's guidelines. NG108-15 cells were marked with a working solution of 50 µM CellTracker™ Blue CMAC (Invitrogen) in complete growth medium, while S16 cells were tracked with a working solution of 5 µM CellTracker™ Deep Red Dye (Invitrogen) in complete growth medium. Prior to scaffold seeding, cells were incubated for 30 to 45 min in their respective CellTracker solution at 37°C in a humidified atmosphere with 5% CO_2 (Forma Series II, ThermoFisher). Afterwards, cells were centrifuged and re-suspended in fresh growth medium prior to seeding in scaffolds. Epifluorescence microscopy (EVOS FL Auto, Life Technologies) was used to visualize scaffolds with stained cells within 72 h, with images of complete scaffold (stitching scan) taken at 24, 48, and 72 h post-seeding. As imaging of stained cells within a three-dimensional biomaterial presents challenges due to intra-material diffusion; thus, the focal plane was strategically centralized to mitigate fluorescence-related aberrations across various planes and facilitate cellular analysis deep within the scaffold. Comprehensive scans were performed on the entirety of the scaffolds to guarantee representative analysis. These experiments were conducted at least thrice, each time in triplicate.

After a 72-h incubation period, the LIVE/DEAD™ Viability/Cytotoxicity Kit (Invitrogen) was used to differentiate live cells from dead ones, as per the manufacturer's instructions. In brief, cell-seeded samples were first rinsed with PBS 1× and then stained with ethidium homodimer-1 and calcein AM dissolved in PBS 1× for 45 min at room temperature in a dark environment. Automated scans were subsequently performed on each specimen at 4× magnification using fluorescence microscopy (EVOS FL Auto, Life Technologies). These experiments were also conducted at least thrice, in triplicate.

From the scans, the viability ratio was determined as the global green fluorescence over the red fluorescence. Briefly, a calculation based on the sum of each colored pixel (red or green) normalized to the total number of pixels analyzed was performed using a Python-based routine leveraging the scikit-image package.[55] Viability was subsequently determined as the ratio between the average green intensity and the average red intensity. Before utilizing the ratio analysis software, the images underwent extensive cleaning to minimize background interference. All images received the same post-treatment.

Immunolabelling of neuronal cells, Schwann cells, and cocultures

Following a total incubation period of 7 days, cell seeded-scaffolds were initially washed thrice with PBS 1×, and then fixed with a 4% (w/v) solution of paraformaldehyde for a duration of 20 min at room temperature. Next, permeabilization was carried out with a 0.5% (v/v) solution of Triton™ X-100 (Millipore-Sigma) in PBS 1× for 10 min. To block non-specific sites, samples were incubated for 1h at 37°C with a 10% (v/v) Normal Goat Serum (NGS) in PBS 1×. This was followed by two washes with PBS 1×. The cultures were then incubated overnight at 4°C with polyclonal S100β (E7C3A) Rabbit mAb 90393 (1:500 dilution) and/or β3-Tubulin (TU-20) Mouse mAb #4466 (1:200 dilution), markers for Schwann cells and neurons respectively. These markers were diluted in 10% (v/v) NGS in PBS 1× and the incubation was conducted on a mechanical stirrer plate at low intensity. Post incubation, the cell cultures were washed thrice with PBS 1× before subjecting them to a second incubation with secondary antibodies and Hoechst 33342 (ThermoFisher) (1:2000 dilution), in sterile PBS 1× containing 10% (v/v) NGS for 90 min at 37°C in a humidified incubator (5% CO_2) under gentle agitation. The secondary antibodies included Anti-rabbit IgG (H+L), F(ab')2 Fragment (Alexa Fluor® 488 Conjugate Green) #4412 (1:500 dilution), and Anti-mouse IgG (H+L), F(ab')2 Fragment (Alexa Fluor® 647 Conjugate) #4410 (1:500 dilution). Stained cells were kept in fresh PBS 1× and visualized at magnifications of 4×, 10×, and 40× with an EVOS FL Auto epifluorescence microscope (Life Technologies).

Statistical methods

Analysis of variance (ANOVA) and post hoc tests (i.e. Tukey's multiple comparison test) were performed to extract meaningful statistical results using statsmodels (0.14.1)[56] Python Library.

Results

Biomaterials fabrication

Neuronal cells require support to function optimally, and biomaterials can fulfill this role. The process of inducing vertical ice crystal formation through unidirectional freeze-casting resulted in frozen scaffolds exhibiting distinct characteristics. Scanning Electron Microscope (SEM) images of transverse cross-sections corroborated the essential physiological attributes required for the experiments, showcasing extensively porous scaffolds with a lamellar pore arrangement and longitudinally aligned micro-channels (75–10 µm), a hallmark of freeze-casting of collagen-rich structures. This structure's significance lies in its crucial role in the success of the biological experimentation, as it emulates the human nerve's physiology, enabling cell colonization and alignement along the biomaterial akin to *in vivo* observations. SEM microscopy images of each batch of the 80/20 collagen/chitosan composite were captured to validate the structure's integrity before their utilization as scaffolds for biological experimentation. This technique was further investigated in a previous article.[51] SEM images seen in Figure 2 confirmed the biomaterials employed in this study share a similar configuration. Therefore, this biomaterial was considered an effective mimetic support for studying the cellular behavior of our coculture.

Cellular behavior in static conditions

Cell colonization via CellTracker™. First, we assessed whether our coculture can effectively colonize small size scaffold segments under static culture conditions. We tested different pre-colonization times of the biomaterials with Schwann cells (data not shown) to determine if there was any impact on cell viability and distribution within the biomaterials. However, no conclusive results emerged from these tests, so it was decided to seed both cell types simultaneously to simplify the process.

CellTracker™ staining served as a tool to distinguish between the two cell types during scaffold colonization, as observed through fluorescence microscopy. Although the fluorescence colors from CellTracker™ exhibit some diffusion within the biomaterial, Figure 3 demonstrates that both cell types effectively colonized small segments of scaffolds within 48 h. Various ratios (neuronal cells: Schwann cells), including 1:1, 1:2, 1:3, 1:10, 1:50, and 1:100, were investigated. The results indicated that ratios

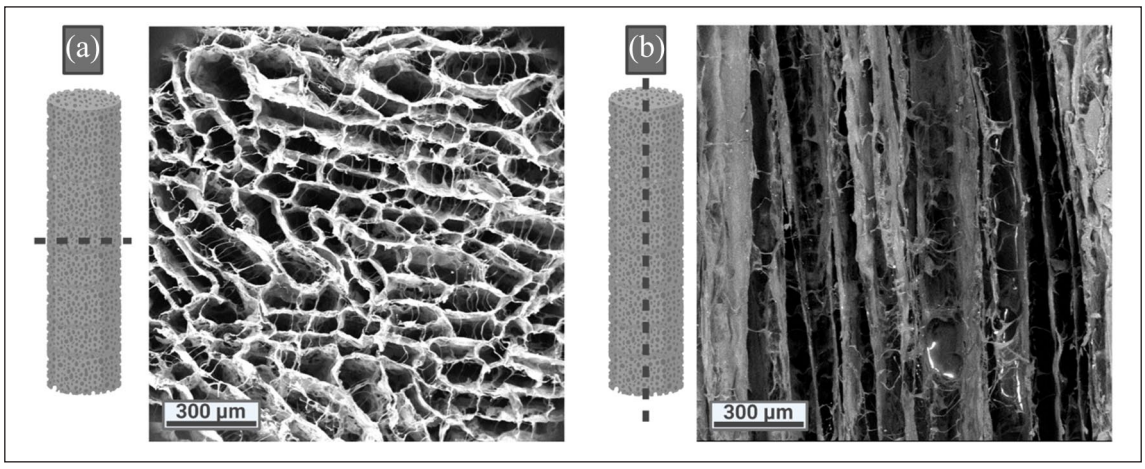

Figure 2. Representative SEM images showing (a) transversal and (b) longitudinal sections of freeze-dried scaffolds of 80/20 [collagen/chitosan] composite with crosslinking treatment ($n = 3$, $N = 9$).

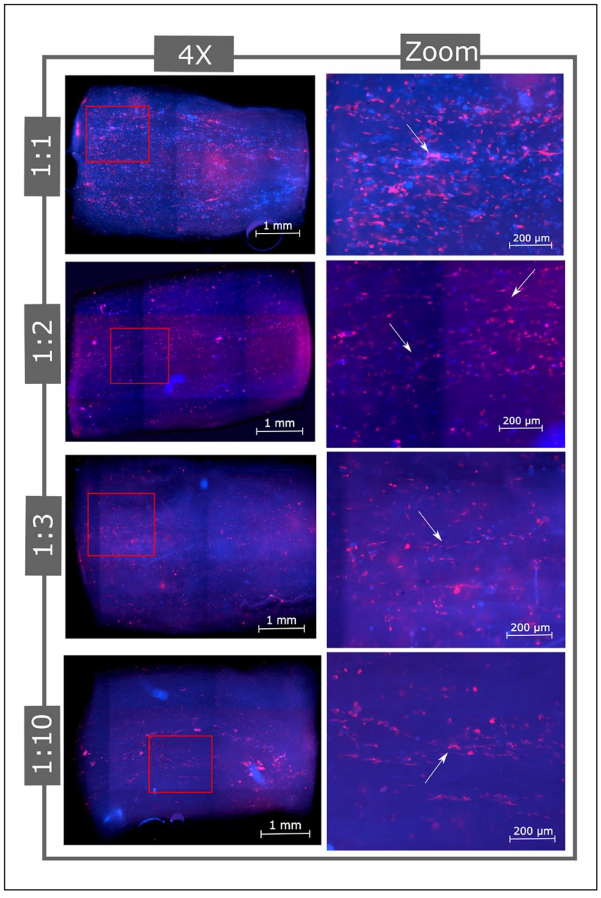

Figure 3. Representative scans and corresponding magnified (Zoom, 4×) images obtained from epifluorescence imaging of CellTracker™ staining after 48 h of incubation in static condition showing NG108-15 (blue) and/or S16 (red) cells cultured (coculture ratio [NG108-15:S16]) on crosslinked scaffolds segments (L = 5 mm, ϕ = 5 mm, 80/20 [collagen/chitosan]) coated with laminins. White arrows show the presence of channel colonization alignment and colocalization of both cell type. ($n = 5$, $N = 15$).

of 1:10 and higher were unable to achieve homogeneous scaffold colonization. Ratios of 1:10, 1:50 (not shown), and 1:100 (not shown) show significantly less cell co-localization, an undesirable outcome for subsequent experiments as our intention was to facilitate interaction between them.

The ratios 1:1, 1:2, and 1:3 demonstrated that both cellular types effectively colonized the scaffold homogeneously with a high cellular density, thereby occupying mostly the entirety of multiple micro-channels and forming a distinctive alignment discernible at a 10× magnification. While visual characteristics appeared comparable among the 1:1, 1:2, and 1:3 ratios, the 1:1 ratio suggests the seeding presence of a greater cell quantity, potentially compromising cellular homogeneity within the channels. Conversely, ratios 1:2 and 1:3 indicate a more homogeneous and balanced seeding of the two cellular types.

It is noteworthy that NG108-15 cells (stained in blue) exhibited, on average, slightly larger and rounder morphologies, potentially encountering challenges in adhering to the channel surfaces individually. In contrast, S16 cells (stained in red) displayed a more elongated morphology, and appeared to colonize more effectively the channel walls along the direction of the microchannels.

In summary, CellTracker™ enabled the visualization of colonization and allowed us to establish that homogeneous colonization of the biomaterial is achievable with a ratio of 1:2. The 1:2 ratio was selected over 1:1 and 1:3 due to negligible qualitative differences, thereby standardizing the methodology and simplifying comparative assessments. This condition was used for the rest of the study.

Cell viability via LIVE/DEAD™ imaging. After confirming colonization, we aimed to ensure that our coculture could survive within our biomaterial. Cells were stained with LIVE-DEAD™ after 7 days post-seeding and revealed with fluorescence microscopy to assess the general cell

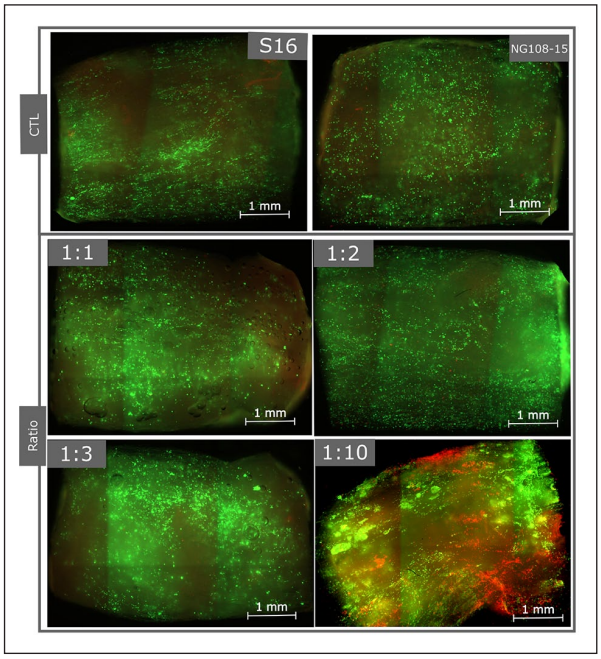

Figure 4. Representative scans and corresponding magnified images obtained from epifluorescence of Live (green)/Dead (red) assays after 7 days of incubation for different NG108-15/S16 ratios cultured on crosslinked scaffolds segments (L = 5 mm, ϕ = 5 mm, 80/20 [collagen/chitosan]) coated with laminins ($n = 5$, $N = 15$).

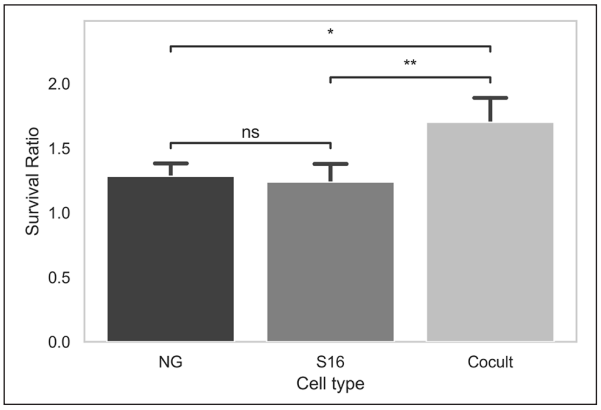

Figure 5. Representative survival ratios (Live cells/Dead cells) analysis after epifluorescence imaging of Live (green)/Dead (red) assays on colonized (coculture ratio 1:2 [NG108-15:S16]) crosslinked scaffolds segments (L = 5 mm, ϕ = 5 mm, 80/20 [collagen/chitosan]) coated with laminins after 7 days of incubation. ($n = 5$, $N = 15$) Only differences with $P \leq 0.05$ were considered statistically significant (ns $p > 0.05$, $*p \leq 0.05$, $**p \leq 0.01$).

viability. Figure 4 displays a representative epifluorescence microscopy scan of the center of a complete scaffold segment showing live cells (in green) and dead cells (in red). It was revealed that coculture cells cultivated in direct contact with the scaffolds exhibited predominantly viable cells (green), with noticeably fewer non-viable cells (red), as depicted in Figure 4. Ratios of 1:1, 1:2, and 1:3 showed a better homogeneity in the colonization and a higher viability. Furthermore, ratios of 1:10 and more diluted expressed more cellular aggregates, which inevitably compromises their viability. Cell viability was visibly similar among ratios 1:1, 1:2, and 1:3 in general.

Even if the control groups (CTL) did not appear to visually exhibit a significant difference in viability, they were visually less successful in uniformly colonizing the scaffolds. Indeed, we observed that the S16 control faced challenges in colonizing the entire scaffold, even though the colonization of the channels was visually apparent. On the other hand, the NG108-15 control demonstrated the formation of aggregates within the channels, a phenomenon observed when NG108-15 cells are seeded alone on surfaces with challenging adhesion, such as biomaterials due to their cancerous characteristics.[57,58] Finally, the lower viabiliy observed for ratios of 1:10 to 1:100 as compared to ratios of 1:1 to 1:3 further confirmed our choice to use the 1:2 ratio for the rest of the study.

We further confirmed those observations by quantifying the normalized green/red ratios (survival ratios) using an image analysis routine. The bar graph in Figure 5 demonstrated that the coculture (ratio 1:2) generally exhibited significantly higher viability ratios compared to monoculture controls, as analyzed from five images drawn from four distinct experiments. The viability of the coculture was significantly different $p \leqslant 0.01$ from the viability of the S16 monoculture. Monoculture of NG108-15 also exhibited a statistically less significant difference $p \leqslant 0.01$.

Cell differentiation assessment via immunostaining. Upon confirming cell viability, we investigated the potential expression of differentiation markers to evaluate their functionality in our biomaterial. S16 cells were labeled with MPZ (green), and NG108-15 cells were labeled with β3-Tubulin (red). These markers are crucial as MPZ is a Schwann cell precursor associated with myelin,[59] and β3-Tubulin (red) plays a role in the growth of specialized nerve cell extensions such as axons and dendrites.[58] We observed that S16 and NG108-15 cells cultivated in direct contact with the scaffolds were also able to express MPZ (green) and β3-Tubulin (red), respectively as shown by Figure 6.

While the MPZ marker was expressed similarly in both the S16 control and coculture, this phenomena did not transposed to the β3-Tubulin marker, which is distinctly less pronounced in its control. Indeed, the presence of pseudoneurites marked in red were clearly discernible in the coculture, as opposed to the NG108-15 control. Coculture also exhibited the most visible alignment and organization of neuronal cells within the

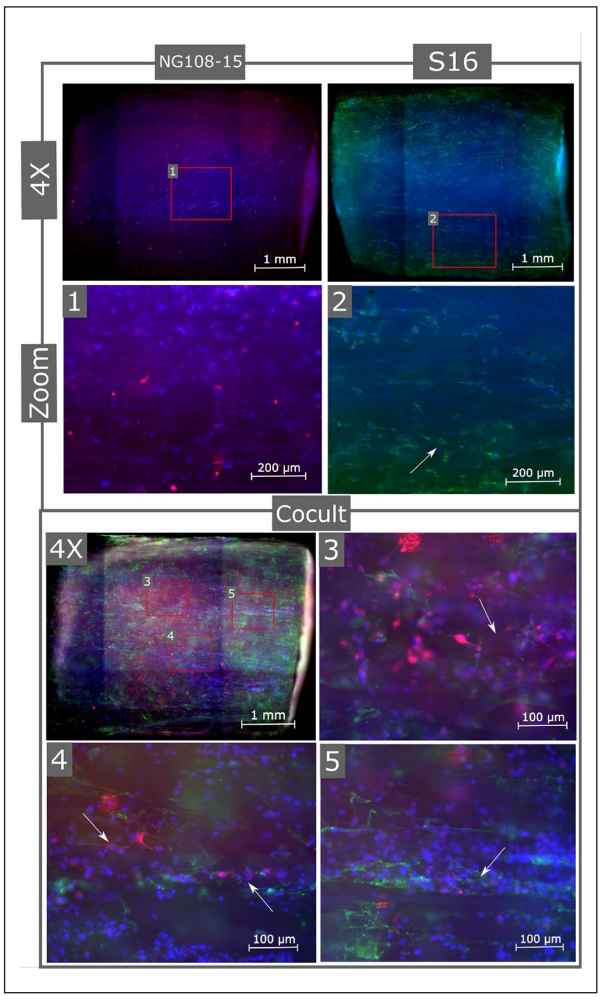

Figure 6. Representative immunostaining scans and pictures with corresponding magnified images of β3-Tubulin (red), MPZ (green), and Hoechst (blue) of colonized NG108-15 and/or S16 cells cultured (coculture ratio 1:2 [NG108-15:S16]) in crosslinked scaffolds segments (L = 5 mm, ϕ = 5 mm, 80/20 [collagen/chitosan]) coated with laminins. White arrows show the presence of complete channel colonization (2 and 5) and the presence of pseudoneurites (3, 4 and 5). Obtained from fluorescence imaging after 7 days of incubation ($n = 3$, $N = 9$).

microchannel structures compared to the NG108-15 control.

In summary, coculture cell morphologies manifested observable alignments in the scaffold microchannels across all conditions. Specific markers for S16 and NG108-15, such as MPZ (green) and β3-Tubulin (red), were present in every conditions but were more prominent in coculture-seeded scaffolds. This is the only condition in which we could observe pseudoneurite formation.

Cellular behavior in dynamic conditions

The seeding ratio of 1:2 (neuronal cells: Schwann cells) and methodological protocols assessed with scaffold segments (5 mm long) was further adapted and carried out with a 30 mm long scaffold. The larger segments were introduced into PDMS culture chambers on a platform that enables a direct perfusion of culture medium to facilitate nutrients and oxygen exchanges. Cells were seeded through an injection port (3-way valve) at one extremity of the scaffold along the direction of the perfusion.

Cell colonization via CellTracker™. The CellTracker™ staining provided insights into the colonization of long scaffold segments. In Figure 7, we observed that the perfusion bioreactor enabled the colonization of the biomaterial along its entire length after 48 h, with a slightly higher concentration of cells at their cell injection extremity. However, a similar colonization pattern was observed for both controls and the coculture, with the coculture appearing to retain a greater quantity of cells overall. Despite the significant diffusion of the blue dye in the biomaterial, it was still possible to observe the presence of both cell types colocalized in many micro-channels of the biomaterial.

Cell viability via LIVE/DEAD™ assay. In terms of viability study, Figure 8 illustrates LIVE-DEAD™ stained cells under epifluorescence microscopy after 7 days of incubation. To evaluate the perfusion's effect on overall cell viability, cell seeding was performed at one end of the scaffold within the culture chamber as described previously. As opposed to dynamic conditions, static condition scaffolds (controls) were further removed from the culture chamber and placed withing a 6-well plate submerged in culture medium. Upon first examination of the results, a noticeable disparity in viability was observed between the static condition (shown in Figure 8(a), where cells were injected at one extremity and cultured in a 6-well plate under static conditions) and the dynamic conditions (depicted in Figure 8(b), where the scaffolds were continuously perfused). It is worth mentioning that the biomaterials are fully colonized, although not uniformly, regardless of variations in cell density within the sample. The dynamic conditions exhibited significantly higher viability compared to their static counterpart. In contrast to the 5 mm static counterpart, the biomaterials seeded as shown in Figure 8(a) exhibited practically no presence of cells under conditions without dynamic perfusion.

As depicted in Figure 8(b), it was interesting to note that cocultured cells cultivated in direct contact with the scaffolds were visibly predominantly viable (green) after 7 days, with considerably fewer non-viable cells (red) even when compared to the controls (S16, NG108-15). When assessing homogeneity in cell viability, there were more areas of necrosis at the ends of the scaffolds. Nonetheless, the interior of the biomaterials still exhibited good overall viability.

Regarding the comparison of the apparent viability as shown in Figure 9, the differences were extremely significant between the biomaterials in Figure 8(a) under static

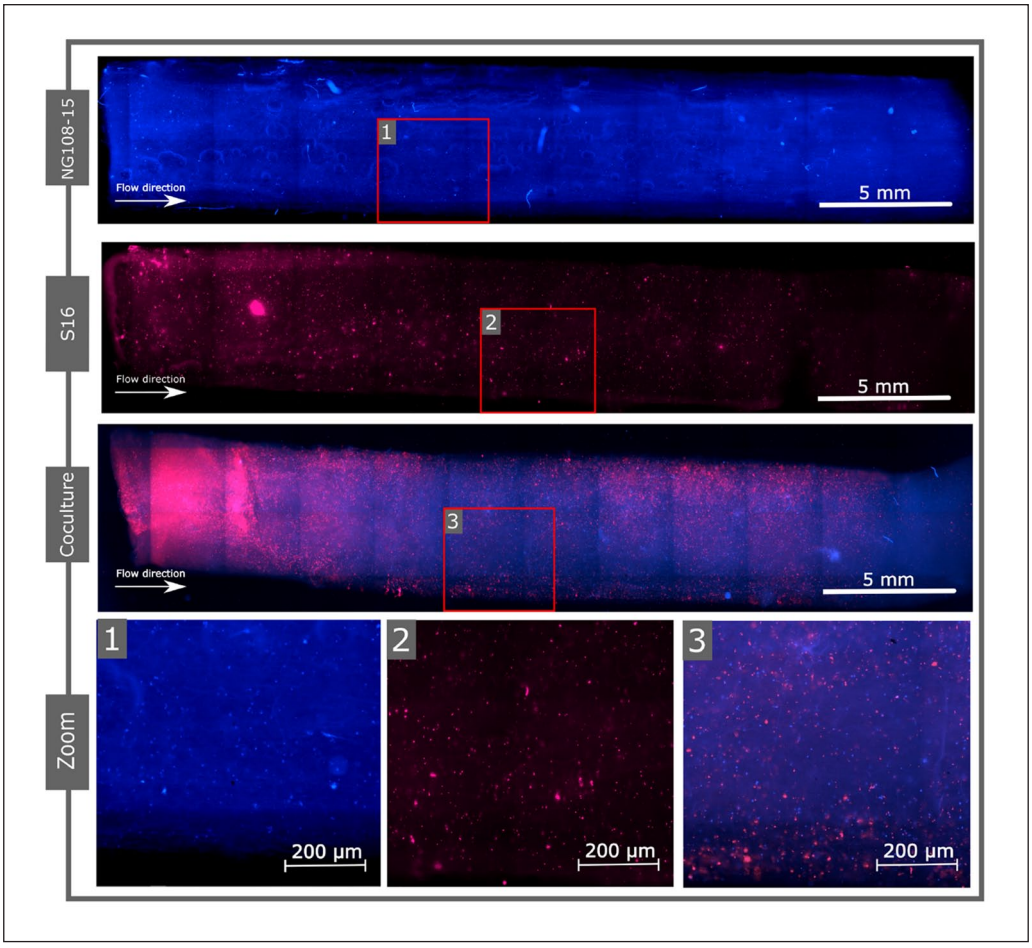

Figure 7. Representative scans and corresponding magnified images obtained from fluorescence imaging of CellTracker™ staining after 48 h of incubation in dynamic condition showing NG108-15 and/or S16 cells cultured (coculture ratio 1:2 [NG108-15:S16]) on crosslinked scaffolds (L = 30 mm, ϕ = 5 mm, 80/20 [collagen/chitosan]) coated with laminins ($n = 4$).

conditions and the biomaterials in Figure 8(b) under dynamic conditions, demonstrating that the viability ratio for NG108-15 $(p \leq 0.001)$ and the coculture $(p \leq 0.0001)$ were nearly 10 times higher and close to five times higher for S16 $(p \leq 0.01)$. It is interesting to note that the S16 cells and the coculture had nearly twice the viability in static condition when compared to the NG108-15 control.

Also, we noticed that the coculture sample had a significantly higher viability than our controls in Figure 9, which was not as pronounced as in static tests in Figure 5. Upon using the same image analysis routine as previously described, the statistics revealed that the viability ratio in the coculture sample was significantly higher $(p \leq 0.0001)$ than the control groups in Figure 9, with a viability ratio nearly twice as high as the monocultures, as determined by the analysis of five images from three independent experiments. Similarly, the dynamic environment of each condition provided significantly higher viability than its static counterpart, with a p-value of $p \leq 0.0001$ for the coculture, $p \leq 0.01$ for S16 cells, and $p \leq 0.001$ for NG108-15 cells. This corresponds to what we observed in Figure 8, thus validating the visual observations of the images produced during fluorescence imaging.

Cell differentiation via immunostaining. Similar to the functionality study conducted at the static level, we used immunostaining to visualize the presence of differentiation factors. Regarding immunostaining in the 30 mm-long biomaterials, it was challenging to obtain high-quality images as the immunomarkers struggled to penetrate the entire biomaterial. The best results were achieved when the biomaterials were removed from the bioreactor after 7 days post-seeding and sectioned into 5 mm-long segments prior to immunostaining. Segments were then subjected to immunolabeling. Given the necessary manipulations of the biomaterials before labeling, which could potentially compromise some structures or harm the final cultivated cells, the images and the specific markers may not be as clear as those obtained during immunostaining in static conditions when the biomaterials were already cut into 5 mm sections before seeding.

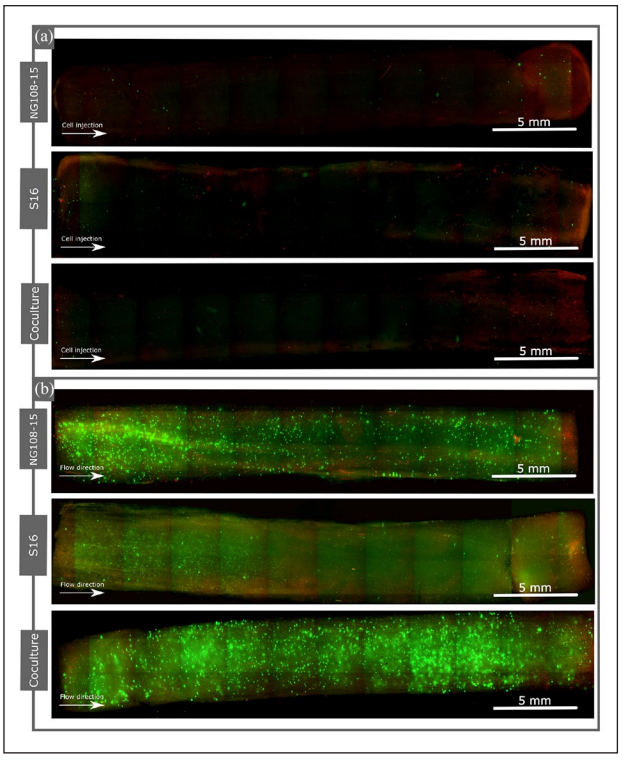

Figure 8. Representative scans of (a) static condition and (b) dynamic condition crosslinked scaffolds (L = 30 mm, ϕ = 5 mm, 80/20 [collagen/chitosan]) coated with laminins. Obtained from epifluorescence imaging with Live (green)/Dead (red) assays after 7 days of incubation showing NG108-15 and/or S16 cells cultured (coculture ratio 1:2 [NG108-15:S16]) (n = 5).

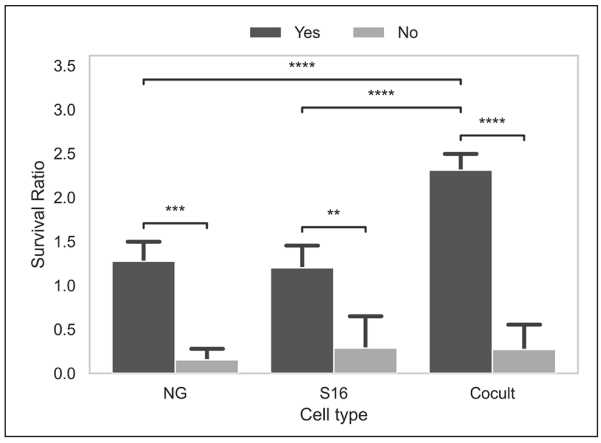

Figure 9. Representative survival ratios (Live cells/Dead cells) obtained from Python ratio analysis routine after epifluorescence imaging of Live(green)/Dead(red) assays of colonized (coculture ratio 1:2 [NG108-15:S16]) crosslinked scaffolds (L = 30 mm, ϕ = 5 mm, 80/20 [collagen/chitosan]) coated with laminins after 7 days of incubation. Yes = incubation with dynamic condition with perfusion bioreactor and No = incubation with static condition in a 6 well plate (Results of static condition are representative of n = 3, N = 9 and dynamic condition are representative of n = 5, N = 15). Only differences with $P \leq 0.05$ were considered statistically significant ($**p \leq 0.01$, $***p \leq 0.001$, $****p \leq 0.0001$).

However, Figure 10 allowed a representative overview of the immunostaining results for cells co-cultured under perfusion. S16 cells were stained for MPZ (green), and NG108-15 cells were stained for β3-Tubulin (red). Specifically, the MPZ marker was expressed similarly in both the S16 control and coculture. For the β3-Tubulin marker, similarly to the results obtained under static culture conditions, the marker was distinctly less pronounced in its controls. However, while we might not discern as many or as distinctly defined pseudoneurites as observed in the static samples, it remained possible to identify some pseudoneurites in the images associated with the coculture. Finally, in accordance with the results in static condition, the coculture also exhibited the most visible alignments and (neurites for NG108-15 and cell bodies for S16) organization within the micro-channel structures as compared to the controls.

Discussion

In this study, large size collagen/chitosan biomaterials (30 mm length, 5 mm diameter, 80/20 [collagen/chitosan]) coated with laminins were mounted into a custom-made perfusion bioreactor to make an *in vitro* model aiming to study peripheral nerve regeneration. Cocultured mouse neurons (NG108-15) and rat Schwann cells (S16) cell lines were studied when exposed to the biomaterial in a three-dimension dynamic environment. Complete colonization, organized cells functionality and good general viability, either individually or together as neuronal-glial cocultures, were found in 30 mm-long biomaterials which has never been reported yet in such a big scale in the context of peripheral nerve applications.

The fabrication of the biomaterial used for experiment was done by a specially designed unidirectional freeze-casting setup, as previously reported in Monfette et al.,[51] to induce vertical ice crystal formation within longitudinally frozen scaffolds. Composite blend of 80/20 [collagen/chitosan] combined with EDC/NHS crosslinking, based on optimal parameters mentioned in other studies,[60,61] were proved to have the best mechanical properties. Furthermore, laminins were added to these biomaterials to enhance cells compatibility and attachment as demonstrate in Monfette et al.[51] The utilization of cells models such as NG108-15 and S16 cell lines are commonly used in study in the field of peripheral nerve research.[41,50] The cell types utilized, including NG108-15 and S16, serve as suitable cell lines for proof of concept. NG108-15, in particular, has been employed as a neuronal model in various studies requiring neuronal differentiation,[57,62,63] some of which involved coculture with Schwann cell models.[58,64]

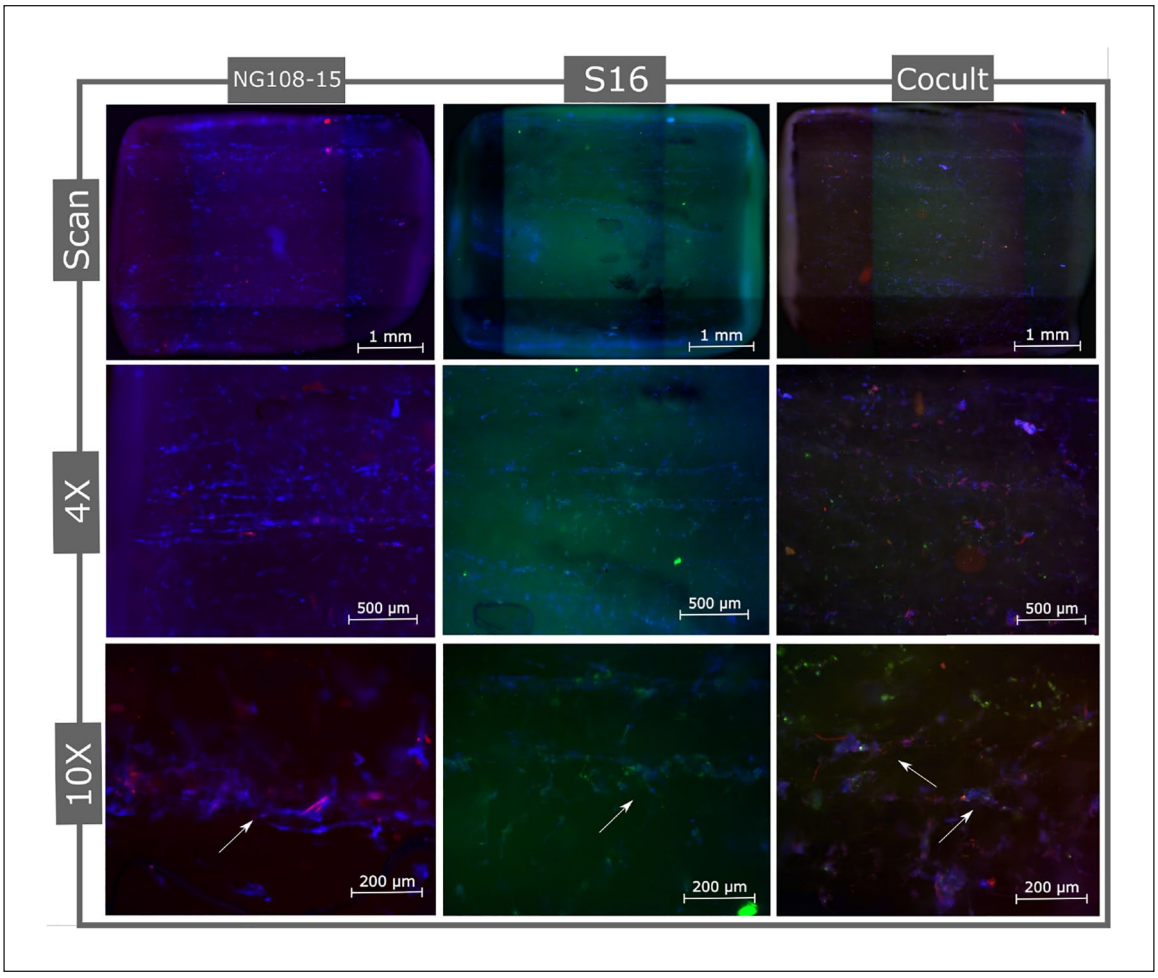

Figure 10. Representative immunostaining scans with corresponding magnified images of β3-Tubulin (red), MPZ (green), and Hoechst (blue) of colonized NG108-15 and/or S16 cells cultured (coculture ratio 1:2 [NG108-15:S16]) in full size crosslinked scaffolds (L = 30 mm, ϕ = 5 mm, 80/20 [collagen/chitosan]) cut into sections (L = 5 mm) coated with laminins. White arrows show the presence of interesting marker localisations. Obtained from epifluorescence imaging after 7 days of incubation ($n = 3$).

Coculture survival, colonization, and differentiation at the contact of the scaffolds in static environment

The static environment allowed us to draw general conclusions about the ability of coculture to coexist in contact with the collagen and chitosan composite biomaterial used. Indeed, static three-dimension conditions enabled us to establish that cocultures in small scaffold segments with more balanced ratios yielded the best experimental outcomes. Although this finding does not fully align with observations in nature, where disparate ratios of up to one myelinating Schwann cell per 1 mm of neurons are observed,[65] more balanced ratios, such as 1:1[50] to 1:10,[66,67] is often employed in laboratory settings for *in vitro* proof-of-concept studies. These more balanced ratios maximize interactions between the two cell types to extract the maximum synergy, as we reported in this study. We demonstrated that colonization, viability, and differentiation were possible under such conditions for segments of 5 mm in length. However, when increasing the useful size of the biomaterial, cellular behavior, such as viability, drastically declined. This phenomenon is expected, as the static environment allows minimal mass transfer, imposing significant limitations on nutrient utilization for cells residing within the biomaterial. Nonetheless, the preliminary use of static three-dimension conditions facilitated the optimization of coculture on a small scale, enabling a smooth transition to the dynamic environment.

Regarding the specific viability of different cell types, assessing the viability of individual cell types within a scaffold containing two cocultured cell types is challenging due to the difficulty in distinguishing between the population. Traditional viability assays cannot differentiate between these cell types, necessitating specific viability markers and efficient cell extraction methods without disruption. This requires sorting based on specific markers and viability analysis, such as flow cytometry. To date, this

comprehensive analysis has not been conducted in the literature for Schwann cell/neuronal cell coculture in three-dimension scaffolds due to extraction complexities. However, CellTracker™ images offered insights into biomaterial distribution and colonization during the initial 72-h post-seeding period.

The optimized results observed during coculture may possibly be explained by the natural role of Schwann cells coexisting with damaged neurons, particularly through their contribution to Wallerian degeneration[23,24] and their ability to differentiate into repair specialists.[68,69] Indeed, during the standard repair mechanism, Schwann cells systematically arrange themselves into formations known as Büngner bands, fostering the growth and guidance of axons.[70] Scaffolds featuring microchannels that are pre-seeded with Schwann cells have demonstrated the ability to mimic these alignments, effectively facilitating the infiltration and regeneration of axons within three-dimension scaffolds.[71,72] The observed structure and cellular arrangement closely resemble what we have witnessed, underscoring the material's anisotropy as a critical factor in the regeneration of nerve tissue in accordance with Monfette et al.[51] Ultimately, it has been repeatedly demonstrated that, in close contact, Schwann cells can secrete growth factors and molecules (such as NGF, BDNF et GDNF) promoting the growth of neurons and their axons[26–28,73] and contribute to axon myelination.[74] Consequently, our results and scientific literature strongly suggests that the coculture of Schwann cells with neurons is associated with enhanced outcomes.

Additionally, interesting results observed in Figure 5 lead to the conclusion that coculture is capable of achieving better viability ratios than the respective controls. Furthermore, as illustrated by the static culture results in Figure 6, the cocultured Schwann cells and neurons demonstrated an enhanced capacity to colonize the biomaterial, achieving superior overall viability and exhibiting more pronounced expression of differentiation markers, such as β3-Tubulin, compared to the control groups. We also observed that coculture enabled better homogeneous colonization of the biomaterial channels and a more pronounced expression of β3-Tubulin associated with pseudoneurites. This finding is consistent with the literature,[39,41] which demonstrates that neuronal cells, when cocultured with Schwann cells, exhibit enhanced expression of β3-Tubulin associated with pseudoneurites compared to their monoculture counterparts.

To evaluate Schwann cell early onsets of differentiation, we also assessed the expression of MPZ in S16 cells seeded in scaffolds. This protein exhibits exclusive expression in Schwann cells within the peripheral nervous system and encodes a type I transmembrane glycoprotein. MPZ is a useful marker for differentiating Schwann cells because of its stage-specific expression pattern, its importance in myelin structure and nerve function, and its ability to help distinguish Schwann cells from other cell types.[59] In this study, we observed a strong expression of MPZ in almost every condition, indicating that Schwann cells can function effectively within this *in vitro* model.

Establishment of an in vitro peripheral nervous system model in a three-dimensional dynamic environment

To enhance the exploration of biomaterial-incorporated three-dimension cell cultures, bioreactor system encompassing crucial components aimed at enhancing reproducibility: temperature and O_2 parameters measurement and control, a replicable and uniform cell seeding process and the opportunity for parallelization, such as simultaneously testing multiple conditions within a single experiment.

In pursuit of a more clinically relevant model for the study of biomaterial-integrated three-dimensional cell cultures, we employed a perfusion bioreactor system. This system was meticulously engineered to enhance experimental reproducibility through the precise control and measurement of temperature and O_2 levels, a uniform cell seeding process, and the ability to test various conditions concurrently within a singular experimental framework. The custom-made bioreactor system used in this study enabled rapid and consistent exploration of three-dimension cell cultures, addressing a significant requirement in the field of tissue engineering for scale up to human size.[75,76] Also, employing a perfused bioreactor ensures an optimal nutrient supply such as O_2 and supplements while efficiently eliminating toxic metabolites from the cell culture growth.[76–79]

Indeed, several models related to the PNS integrate coculture with three-dimensional biomaterials,[39,80,81] which has been proven effective but lacks the dynamic key component found in the *in vivo* environment, diminishing the realism of these models. On the other hand, in articles addressing the development of an *in vitro* model under dynamic conditions, the literature often presents perspectives different from our bioreactor technology. Many articles on the subject utilize microfluidic technologies,[48,49] operating at a smaller scale compared to what is found *in vivo*, which could pose challenges when scaling up for human applications. Despite the advantages of microfluidics,[47] the unique and compelling scale of our model distinguishes it from the literature. When exploring *in vitro* models developing bioreactors for clinical-scale tissue engineering, articles such as Piola et al.,[82] Parrish et al.,[83] and Wendt et al.[84] are found. While not specialized for the PNS, they offer a more comprehensive approach to tissue engineering.

The only models that align with the characteristics of our model would be the model by Sun et al.[85] The study utilized a closed-loop bioreactor system with the capability to evaluate novel tissue-engineered peripheral nerve conduits *in vitro*, with cell cultures carried out for 4 days.

This system integrates a completely closed system, allowing for easy operation under sterile conditions and the potential for the parallel operation of individual chambers for simultaneous and comparable experiments. It also explores the possibility of testing synthetic microfibers aligned with viscose rayon and polystyrene, obtained through electrospinning. It is interesting to note that the conclusions of the study regarding the crucial role of the dynamic environment are remarkably similar to the conclusions in the current article, namely, higher cellular viability and significantly greatercolonisation of the biomaterials compared to static culture. However, this study was conducted several years ago, and technologies have imposed several limitations on the model. Firstly, the biomaterial used was not as efficient as ours,[51] the distribution of viable cells along the scaffolds was highly uneven, especially toward the open end of longer scaffolds (30–80 mm). There was also a significant decrease in cell viability and cell count with higher and less well-controlled fluid flow rates compared to our system, which utilizes a high-precision micro-peristaltic stepper motor capable of delivering smaller flow rates with high accuracy.

Coculture survival, colonization, and differentiation at the contact of the scaffolds in dynamic environment

The static environment provides limited opportunities for material transfer to cell cultures. Consequently, lower cellular viability is expected in an environment where nutrients circulate less efficiently, aligning well with the overall results of the experiments presented in this article. Beyond material transfer, the perfusion rate may represent a crucial aspect in the experimental outcomes. Indeed, the ultimate goal is to replicate the human environment as effectively as possible; however, humans exhibit multiple variations not only among individuals but also within their own organisms.[86] Therefore, finding a perfusion rate that exactly simulates what one might achieve in humans is extremely challenging. The choice of the perfusion rate aligns with similar studies on the subject. The flow rates used in this study were 10, 50, 150, and 200 µL/min, with the majority of experiments conducted at 150 µL/min, based on parameters found in the literature concerning the peripheral nervous system, for example: 10 to 250 µL/min for Schmid et al.,[53] 13.3, 50, and 83.3 µL/min for Sun et al.,[85] 12, 120, and 600 µL/min for Campos Marín,[36] and 30 to 100 µL/min for Piola et al.[82] The variation in flow rates in our case had no visible impact on colonization. The only noticeable observation was the loss of cell density when flow rates exceed 250 µL/min, probably due to the fact that cells with weaker adhesion to the biomaterial were more easily washed away, and there was a relatively high degree of shear force considering the small size of the micro-channels.[85] Nevertheless, it was interesting to observe the impact of material transfer and perfusion in different experimental stages.

In terms of colonization, both the coculture and the control groups have demonstrated effective colonization of the biomaterial under perfusion as opposed to unperfused scaffolds. It is noteworthy to mention that the coculture seemed to positively influence the overall distribution of cells within the biomaterial, resulting in a higher cellular density retained in the biomaterial, a phenomenon also observed in static experiments. This phenomenon may be attributed to an interaction between the two cell types. This interaction have been reported in articles such as Hyung et al.[34] and Malheiro et al.[39] This could be a potentially interesting aspect to investigate more deeply in future studies. Another observation from the results in Figure 7 indicates a higher cellular density upstream of the biomaterial, which might be attributed to the seeding process. Cells were initially seeded at one end of the biomaterial. After 48 h of incubation, CellTracker™ images were captured. From our observations, it appeared that some cells may not have had enough time to migrate to the biomaterial's deeper zones within this period. This was further supported by the increased homogeneity in cell distribution observed after 7 days (168 h), as indicated by the Live/Dead™ cell assay results. The seeding process's flow rate may have an impact, as evidenced by studies that have experimented with various seeding flow rates.[36] We found that slightly reducing the seeding flow rate may have helped diminish shear forces, thereby improving viability, although not significantly.

The conclusions in link with the viability were arguably the most interesting in this study. What is the most noteworthy is the dynamic environment's ability to significantly enhance the coculture viability in full-scale biomaterials with a length of 30 mm, a phenomenon not yet reported to the best of our knowledge. As indicated by the results obtained with Live/Dead™ fluorescence data, in the absence of this dynamic environment, none of the cell types can attain satisfactory viability nor colonization. This implies that perfusion is indeed the cause of the significantly greater viability and cell colonization observed in the biomaterial.[53,77] The viability over several days has been documented in Campbell et al.[87] They demonstrated that a coculture could persist for at least 21 days, and myelin sheaths formed around axonal fibers from day 14 onwards. Similarly, in the coculture of primary motor neurons and Schwann cells,[34] observed a considerable improvement in the viability of motor neurons compared to motor neuron monoculture. While the vast majority of neurons in monoculture failed to survive, the coculture showed almost no cell death up to 21 days of culture.

Regarding the immunostaining results on the biomaterials under dynamic conditions in the 30 mm-long biomaterials, despite the challenging task of obtaining high-quality images due to the immunomarkers struggling

to penetrate the entire biomaterial and necessary manipulations with the biomaterials before labeling, which likely impacted the labeling quality, we still observed a positive presence of MPZ and β3-Tubulin markers. This corresponds with the results obtained in the static environment. A practically identical presence of the MPZ marker is observed both in static and dynamic conditions. The main distinction lies in the fact that pseudoneurites aligned along the microchannels were only observable under coculture conditions, emphasizing the significance of coculture. Despite the pseudoneurites being less discernible in the zoomed images of dynamic results due to lower quality compared to static results, a similarly apparent presence of the β3-Tubulin marker is observed, with a distinction in the concentration of the marker in structures resembling pseudoneurites in the coculture images. In a related study Daud et al.,[41] investigated the development of a three-dimension *in vitro* peripheral nerve model using aligned electrospun polycaprolactone fiber scaffolds to explore neurite guidance, cell viability, and cellular organization in neuronal-glial cocultures. They demonstrated that NG108-15 neuronal cell neurites extended up to 2.50 mm after 10 days of culture on 1 mm diameter fibers in serum-free DMEM containing specific supplements. A 7–10 day incubation period for a coculture in contact with a biomaterial is not very long, but remain standard in many studies.[46,53,88] This timeframe enables the initiation of physiological changes in neuronal cells, such as the onset of neurite formation and the beginning of maturation molecule expression in Schwann cells as we observed. In addition, it provides a reasonable timeframe for comparing cocultures in static and dynamic environments.[53] In a future study, we plan to initiate longer coculture incubations to observe late differentiation-related outcomes in the context of coculture. Several studies extend beyond 21 days[48,87] (28 days[89,90]; 40 days[48]), observing more developed neurites and even an onset of myelination.

Finally, various research avenues can be considered to enhance the fidelity of this *in vitro* model replicating the regenerative processes of the PNS. Firstly, extending the coculture period over multiple consecutive weeks would better mimic long-term physiological conditions, providing a more realistic perspective of regenerative processes such as axonal growth of neurons.[91] Moreover, particular attention should be given to the validation of cell functionality, emphasizing crucial aspects such as the ability of Schwann cells to form a myelin sheath, a fundamental step in the nerve regeneration process. Moreover, integrating a greater variety of cellular actors, such as macrophages, and exploring complex interactions between different cellular populations could strengthen the model's validity. Cell types employed in this study, such as NG108-15 and S16, act as good cell lines for proof of concept; however, since these are cell lines derived from rodents, their behavior may differ from that of primary cells, such as DRG. Ultimately, testing human cell lines, animal primary cells, or even stem cells represent promising avenues to enhance the model's representativeness based on the biological complexity inherent to the human organism.

Conclusion

PNI impose substantial health and socio-economic challenges. Understanding PNS regeneration is vital for discovering cost-effective therapeutic strategies. Ethical concerns and high costs linked to animal research have driven researchers to embrace innovative *in vitro* models, proving reliable and reproducible results. This study underscores the importance of incorporating the dynamic aspect in the development of three-dimension *in vitro* models at a clinically relevant scale, which is a novelty in the field. It proposes an effective combination of unique characteristics utilizing coculture, a three-dimension biomimetic scaffold, perfusion bioreactors, and clinical-scale size to replicate environments similar to those found *in vivo*. The biomaterial, optimized with collagen and chitosan, supports Schwann and neuronal cell distribution, while perfusion enhances nutrient availability, oxygen supply, and waste removal. Most importantly, this model enables work on clinically relevant biomaterial scales, showing early differentiation in cocultured cell lines NG108-15 and S16. Ultimately, this study opens new promising avenues for studying and advancing peripheral nerve injury treatments.

Declaration of conflicting interests

The author(s) declared no potential conflicts of interest with respect to the research, authorship, and/or publication of this article.

Funding

The author(s) disclosed receipt of the following financial support for the research, authorship, and/or publication of this article: This work was supported by the Natural Sciences and Engineering Research Council of Canada (grant RGPIN-2019-06055).

ORCID iD

Marc-Antoine Lauzon https://orcid.org/0009-0007-0576-7322

References

1. Taylor CA, Braza D, Rice JB, et al. The incidence of peripheral nerve injury in extremity trauma. *Am J Phys Med* 2008; 87(5): 381–385. DOI: 10.1097/PHM.0b013e318 15e6370.
2. Bruyns CNP, Jaquet JB, Schreuders TAR, et al. Predictors for return to work in patients with median and ulnar nerve injuries. *J Hand Surg Am* 2003; 28(1): 28–34. DOI: 10.1053/jhsu.2003.50026.
3. Velopulos C, Enwerem NY, Obirieze A, et al. National cost of trauma care by payer status. *J Surg Res* 2013; 184(1): 444–449. DOI: 10.1016/j.jss.2013.05.068.

4. Schilling B, Baker J, Komatsu C, et al. Intramuscular injection of skeletal muscle derived extracellular matrix mitigates denervation atrophy after sciatic nerve transection. *J Tissue Eng* 2021; 12: 204173142110324. DOI: 10.1177/20417314211032491.
5. Brattain K. *Analysis of the peripheral nerve repair market in the united states*. Magellan Medical Technology Consultants, Inc, 2013, p. 11.
6. Murphy RNA, de Schoulepnikoff C, Chen JHC, et al. The incidence and management of peripheral nerve injury in England (2005–2020). *J Plast Reconstr Aesthet Surg* 2023; 80: 75–85. DOI: 10.1016/j.bjps.2023.02.017.
7. Dy CJ, Lingampalli N, Peacock K, et al. Direct cost of surgically treated adult traumatic brachial plexus injuries. *J Hand Surg Glob Online* 2020; 2(2): 77–79. DOI: 10.1016/j.jhsg.2019.12.001.
8. Atkins S, Smith KG, Loescher AR, et al. Scarring impedes regeneration at sites of peripheral nerve repair. *NeuroReport* 2006; 17(12): 1245–1249. DOI: 10.1097/01.wnr.0000230519.39456.ea.
9. Siemionow M and Brzezicki G. Chapter 8 current techniques and concepts in peripheral nerve repair. In: *International review of neurobiology*. Academic Press, 2009, Vol. 87, pp. 141–172. DOI: 10.1016/S0074-7742(09)87008-6.
10. Lundborg G and Richard P. Bunge memorial lecture nerve injury and repair—A challenge to the plastic brain. *J Peripher Nerv Sys* 2003; 8(4): 209–226. DOI: 10.1111/j.1085-9489.2003.03027.x.
11. Noble J, Munro CA, Prasad VS, et al. Analysis of upper and lower extremity peripheral nerve injuries in a population of patients with multiple injuries. *J Trauma* 1998; 45(1): 116–122. DOI: 10.1097/00005373-199807000-00025.
12. Ruijs ACJ, Jaquet JB, Kalmijn S, et al. Median and Ulnar nerve injuries: A meta-analysis of predictors of motor and sensory recovery after modern microsurgical nerve repair. *Plast Reconst Surg* 2005; 116(2): 484–494. DOI: 10.1097/01.prs.0000172896.86594.07.
13. Lundborg G and Rydevik B. Effects of stretching the tibial nerve of the rabbit. A preliminary study of the intraneural circulation and the barrier function of the perineurium. *J Bone Joint Surg Br Vol* 1973; 55(2): 390–401.
14. de Medinaceli L, Prayon M and Merle M. Percentage of nerve injuries in which primary repair can be achieved by end-to-end approximation: review of 2,181 nerve lesions. *Microsurgery* 1993; 14(4): 244–246. DOI: 10.1002/micr.1920140406.
15. Baradaran A, El-Hawary H, Efanov JI, et al. Peripheral nerve healing: so near and yet so far. *Semin Plast Surg* 2021; 35(03): 204–210. DOI: 10.1055/s-0041-1731630.
16. Hussain G, Wang J, Rasul A, et al. Current status of therapeutic approaches against peripheral nerve injuries: a detailed story from injury to recovery. *Int J Biol Sci* 2020; 16(1): 116–134. DOI: 10.7150/ijbs.35653.
17. Griffin M, Malahias M, Hindocha S, et al. Peripheral nerve injury: principles for repair and regeneration. *Open Orthop J* 2014; 8(1). DOI: 10.2174/1874325001408010199.
18. Grinsell D and Keating CP. Peripheral nerve reconstruction after injury: A review of clinical and experimental therapies. *BioMed Res Int* 2014; 2014: e698256. DOI: 10.1155/2014/698256.
19. Mauch JT, Bae A, Shubinets V, et al. A Systematic review of sensory outcomes of digital nerve gap reconstruction with autograft, allograft, and conduit. *Ann Plast Surg* 2019; 82(4S Suppl 3): S247–S255. DOI: 10.1097/SAP.0000000000001851
20. Jiang X, Lim SH, Mao HQ, et al. Current applications and future perspectives of artificial nerve conduits. *Exp Neurol* 2010; 223(1): 86–101. DOI: 10.1016/j.expneurol.2009.09.009.
21. Haycock JW. 3D cell culture: a review of current approaches and techniques. *Methods Mol Biol* 2011; 695: 1–15. DOI: 10.1007/978-1-60761-984-0_1.
22. Song D, Yang D, Powell CA, et al. Cell–cell communication: old mystery and new opportunity. *Cell Biol Toxicol* 2019; 35(2): 89–93. DOI: 10.1007/s10565-019-09470-y.
23. Burnett MG and Zager EL. Pathophysiology of peripheral nerve injury: a brief review. *Neurosurg Focus* 2004; 16(5): 1–7. DOI: 10.3171/foc.2004.16.5.2.
24. Chen ZL, Yu WM and Strickland S. Peripheral regeneration. *Ann Rev Neurosci* 2007; 30: 209–233. DOI: 10.1146/annurev.neuro.30.051606.094337.
25. Birch R and Raji AR. Repair of median and ulnar nerves. Primary suture is best. *J Bone Joint Surg Br Vol* 1991; 73(1): 154–157. DOI: 10.1302/0301-620X.73B1.1991753.
26. Schmidt CE and Leach JB. Neural tissue engineering: strategies for repair and regeneration. *Ann Rev Biomed Eng* 2003; 5: 293–347. DOI: 10.1146/annurev.bioeng.5.011303.120731.
27. Gordon T. The role of neurotrophic factors in nerve regeneration. *Neurosurg Focus* 2009; 26(2): E3. DOI: 10.3171/FOC.2009.26.2.E3
28. Belkas JS, Shoichet MS and Midha R. Axonal guidance channels in peripheral nerve regeneration. *Oper Tech Orthop* 2004; 14(3): 190–198. DOI: 10.1053/j.oto.2004.06.001.
29. Dai LG, Huang GS and Hsu SH. Sciatic nerve regeneration by cocultured Schwann cells and stem cells on microporous nerve conduits. *Cell Transplant* 2013; 22(11): 2029–2039. DOI: 10.3727/096368912X658953.
30. van Neerven SGA, Krings L, Haastert-Talini K, et al. Human Schwann cells seeded on a novel collagen-based microstructured nerve guide survive, proliferate, and modify neurite outgrowth. *BioMed Res Int* 2014; 2014: 493823. DOI: 10.1155/2014/493823.
31. Han GH, Peng J, Liu P, et al. Therapeutic strategies for peripheral nerve injury: decellularized nerve conduits and Schwann cell transplantation. *Neural Regen Res* 2019; 14(8): 1343–1351. DOI: 10.4103/1673-5374.253511.
32. Fornaro M, Tos P, Geuna S, et al. Confocal imaging of Schwann-cell migration along muscle-vein combined grafts used to bridge nerve defects in the rat. *Microsurgery* 2001; 21(4): 153–155. DOI: 10.1002/micr.1029.
33. Bozkurt A, Brook GA, Moellers S, et al. In vitro assessment of axonal growth using dorsal root ganglia explants in a novel three-dimensional collagen matrix. *Tissue Eng* 2007; 13(12): 2971–2979. DOI: 10.1089/ten.2007.0116.
34. Hyung S, Yoon Lee B, Park JC, et al. Coculture of primary motor neurons and schwann cells as a model for in vitro myelination. *Sci Rep* 2015; 5: 15122. DOI: 10.1038/srep15122.

35. Yi S, Xu L and Gu X. Scaffolds for peripheral nerve repair and reconstruction. *Exp Neurol* 2019; 319: 112761. DOI: 10.1016/j.expneurol.2018.05.016.
36. Campos Marín A, Brunelli M and Lacroix D. Flow perfusion rate modulates cell deposition onto scaffold substrate during cell seeding. *Biomech Model Mechanobiol* 2018; 17(3): 675–687. DOI: 10.1007/s10237-017-0985-4.
37. Maggiore JC, Burrell JC, Browne KD, et al. Tissue engineered axon-based "living scaffolds" promote survival of spinal cord motor neurons following peripheral nerve repair. *J Tissue Eng Regen Med* 2020; 14(12): 1892–1907. DOI: 10.1002/term.3145.
38. Pawelec K, Yoon C, Giger R, et al. Engineering a platform for nerve regeneration with direct application to nerve repair technology. *Biomaterials* 2019; 216: 119263. DOI: 10.1016/j.biomaterials.2019.119263.
39. Malheiro A, Morgan F, Baker M, et al. A three-dimensional biomimetic peripheral nerve model for drug testing and disease modelling. *Biomaterials* 2020; 257: 120230. DOI: 10.1016/j.biomaterials.2020.120230.
40. Malheiro A, Seijas-Gamardo A, Harichandan A, et al. Development of an in vitro biomimetic peripheral neurovascular platform. *ACS Appl Mater Interfaces* 2022; 14(28): 31567–31585. DOI: 10.1021/acsami.2c03861.
41. Daud MFB, Pawar KC, Claeyssens F, et al. An aligned 3D neuronal-glial co-culture model for peripheral nerve studies. *Biomaterials* 2012; 33(25): 5901–5913. DOI: 10.1016/j.biomaterials.2012.05.008.
42. Valmikinathan CM, Hoffman J and Yu X. Impact of scaffold micro and macro architecture on schwann cell proliferation under dynamic conditions in a rotating wall vessel bioreactor. *Mater Sci Eng C Mater Biol Appl* 2011; 31(1): 22–29. DOI: 10.1016/j.msec.2010.04.001.
43. Osaki T, Sivathanu V and Kamm RD. Engineered 3D vascular and neuronal networks in a microfluidic platform. *Sci Rep* 2018; 8(1): 5168. DOI: 10.1038/s41598-018-23512-1.
44. Augustine R, Aqel AH, Kalva SN, et al. Bioengineered microfluidic blood-brain barrier models in oncology research. *Transl Oncol* 2021; 14(7): 101087. DOI: 10.1016/j.tranon.2021.101087.
45. Cai X, Briggs RG, Homburg HB, et al. Application of microfluidic devices for glioblastoma study: current status and future directions. *Biomed Microdevices* 2020; 22(3): 60. DOI: 10.1007/s10544-020-00516-1.
46. Sharma AD, McCoy L, Jacobs E, et al. Engineering a 3D functional human peripheral nerve in vitro using the nerve-on-a-chip platform. *Sci Rep* 2019; 9: 8921. DOI: 10.1038/s41598-019-45407-5.
47. Holloway PM, Willaime-Morawek S, Siow R, et al. Advances in microfluidic in vitro systems for neurological disease modeling. *J Neurosci Res* 2021; 99(5): 1276–1307. DOI: 10.1002/jnr.24794.
48. Hyung S, Lee SR, Kim J, et al. A 3D disease and regeneration model of peripheral nervous system–on–a–chip. *Sci Adv* 2021; 7(5): eabd9749. DOI: 10.1126/sciadv.abd9749.
49. Yu Y, Jin B, Chen J, et al. Nerve-on-a-chip derived biomimicking microfibers for peripheral nerve regeneration. *Adv Sci* 2023; 10: e2207536. DOI: 10.1002/advs.202207536.
50. Hong WS, Young EWK, Tepp WH, et al. A microscale neuron and Schwann cell coculture model for increasing detection sensitivity of botulinum neurotoxin type A. *Toxicol Sci Off J Soc Toxicol* 2013; 134(1): 64–72. DOI: 10.1093/toxsci/kft082.
51. Monfette V, Choinière W, Godbout-Lavoie C, et al. Thermoelectric freeze-casting of biopolymer blends: Fabrication and characterization of large-size scaffolds for nerve tissue engineering applications. *J Funct Biomater* 2023; 14(6): 330. DOI: 10.3390/jfb14060330.
52. El Kheir W, Dumais A, Beaudoin M, et al. Impact of simulated brain interstitial fluid flow on the chemokine CXCL12 release from an alginate-based hydrogel in a new 3D in vitro model. *Front Drug Deliv* 2023; 3: 1227776. DOI: 10.3389/fddev.2023.1227776.
53. Schmid J, Schwarz S, Meier-Staude R, et al. A perfusion bioreactor system for cell seeding and oxygen-controlled cultivation of three-dimensional cell cultures. *Tissue Eng Part C Methods* 2018; 24(10): 585–595. DOI: 10.1089/ten.TEC.2018.0204.
54. Bell C. CalebBell/thermo, 2024. https://github.com/CalebBell/thermo.Original-date:2016-07-01T16:04:56Z
55. van der Walt S, Schönberger JL, Nunez-Iglesias J, et al. Scikit-image: image processing in Python. *PeerJ* 2014; 2: e453. DOI: 10.7717/peerj.453.
56. Seabold S and Perktold J. Statsmodels: econometric and statistical modeling with python. *Proceedings of the 9th Python in Science Conference*, Austin, June 28–30, 2010, pp. 92–96.
57. Seidman KJN, Barsuk JH, Johnson RF, et al. Differentiation of NG108-15 neuroblastoma cells by serum starvation or dimethyl sulfoxide results in marked differences in angiotensin II receptor subtype expression. *J Neurochem* 1996; 66(3): 1011–1018. DOI: 10.1046/j.1471-4159.1996.66031011.x.
58. Armstrong SJ, Wiberg M, Terenghi G, et al. ECM molecules mediate both Schwann cell proliferation and activation to enhance neurite outgrowth. *Tissue Eng* 2007; 13(12): 2863–2870. DOI: 10.1089/ten.2007.0055.
59. Liu Z, Jin YQ, Chen L, et al. Specific marker expression and cell state of Schwann cells during culture in vitro. *PloS One* 2015; 10(4): e0123278. DOI: 10.1371/journal.pone.0123278
60. Martínez A, Blanco MD, Davidenko N, et al. Tailoring chitosan/collagen scaffolds for tissue engineering: Effect of composition and different crosslinking agents on scaffold properties. *Carbohydr Polym* 2015; 132: 606–619. DOI: 10.1016/j.carbpol.2015.06.084.
61. Bax DV, Davidenko N, Gullberg D, et al. Fundamental insight into the effect of carbodiimide crosslinking on cellular recognition of collagen-based scaffolds. *Acta Biomater* 2017; 49: 218–234. DOI: 10.1016/j.actbio.2016.11.059.
62. Beczkowska I, Gracy K, Pickel V, et al. Detection of delta opioid receptor and N-methyl-D-aspartate receptor-like immunoreactivity in retinoic acid-differentiated neuroblastoma x glioma (NG108-15) cells. *J Neurosci Res* 1997; 47(1): 83–89. DOI: 10.1002/(SICI)1097-4547(19970101)47:1⟨83::AID-JNR9⟩3.0.CO;2-B.
63. Müller D, Greenland KJ, Speth RC, et al. Neuronal differentiation of NG108-15 cells has impact on nitric oxide- and membrane (natriuretic peptide receptor-A) cyclic GMP-generating proteins. *Mol Cell Endocrinol* 2010; 320(1): 118–127. DOI: 10.1016/j.mce.2010.01.022.

64. Kaewkhaw R, Scutt AM and Haycock JW. Anatomical site influences the differentiation of adipose-derived stem cells for Schwann-cell phenotype and function. *Glia* 2011; 59(5): 734–749. DOI: 10.1002/glia.21145.
65. Tortora GJ and Derrickson BH. *Principles of anatomy and physiology*. John Wiley & Sons, 2018. ISBN 978-1-119-44445-9.
66. Park SE, Ahn J, Jeong HE, et al. A three-dimensional in vitro model of the peripheral nervous system. *NPG Asia Mater* 2021; 13(1): 1–11. DOI: 10.1038/s41427-020-00273-w.
67. Päiväläinen S, Nissinen M, Honkanen H, et al. Myelination in mouse dorsal root ganglion/Schwann cell cocultures. *Mol Cell Neurosci* 2008; 37(3): 568–578. DOI: 10.1016/j.mcn.2007.12.005.
68. Gomez-Sanchez JA, Carty L, Iruarrizaga-Lejarreta M, et al. Schwann cell autophagy, myelinophagy, initiates myelin clearance from injured nerves. *J Cell Biol* 2015; 210(1): 153–168. DOI: 10.1083/jcb.201503019.
69. Fu SY and Gordon T. Contributing factors to poor functional recovery after delayed nerve repair: prolonged denervation. *J Neurosci J Soc Neurosci* 1995; 15(5 Pt 2): 3886–3895.
70. Jessen KR, Mirsky R and Lloyd AC. Schwann cells: development and role in nerve repair. *Cold Spring Harb Perspect Biol* 2015; 7(7): a020487. DOI: 10.1101/cshperspect.a020487.
71. Zhou G, Chen Y, Dai F, et al. Chitosan-based nerve guidance conduit with microchannels and nanofibers promotes schwann cells migration and neurite growth. *Colloids Surf B Biointerfaces* 2023; 221: 112929. DOI: 10.1016/j.colsurfb.2022.112929.
72. Liu C, Kray J and Chan C. Schwann cells enhance penetration of regenerated axons into three-dimensional microchannels. *Tissue Eng Regen Med* 2018; 15(3): 351–361. DOI: 10.1007/s13770-018-0115-0.
73. Höke A, Gordon T, Zochodne DW, et al. A decline in glial cell-line-derived neurotrophic factor expression is associated with impaired regeneration after long-term Schwann cell denervation. *Exp Neurol* 2002; 173(1): 77–85. DOI: 10.1006/exnr.2001.7826.
74. Thompson DM and Buettner HM. Oriented Schwann cell monolayers for directed neurite outgrowth. *Ann Biomed Eng* 2004; 32(8): 1120–1130. DOI: 10.1114/b:abme.0000036648.68804.e7.
75. Ravichandran A, Liu Y and Teoh SH. Review: bioreactor design towards generation of relevant engineered tissues: focus on clinical translation. *J Tissue Eng Regen Med* 2018; 12(1): e7–e22. DOI: 10.1002/term.2270.
76. Kasper C, Griensven MV and Pörtner R. *Bioreactor systems for tissue engineering*. Springer Science & Business Media, 2009. ISBN 978-3-540-69356-7.
77. Pörtner R, Nagel-Heyer S, Goepfert C, et al. Bioreactor design for tissue engineering. *J Biosci Bioeng* 2005; 100(3): 235–245. DOI: 10.1263/jbb.100.235.
78. Bancroft GN, Sikavitsas VI and Mikos AG. Design of a flow perfusion bioreactor system for bone tissue-engineering applications. *Tissue Engin* 2003; 9(3): 549–554. DOI: 10.1089/107632703322066723.
79. Schilling BK, Lamberti KK, Snowden MJ, et al. Design and fabrication of an automatable, 3D printed perfusion device for tissue infusion and perfusion engineering. *Tissue Eng Part A* 2020; 26(5–6): 253–264. DOI: 10.1089/ten.tea.2019.0209.
80. Vimal SK, Ahamad N and Katti DS. A simple method for fabrication of electrospun fibers with controlled degree of alignment having potential for nerve regeneration applications. *Mat Sci Eng C* 2016; 63: 616–627. DOI: 10.1016/j.msec.2016.03.008.
81. Fang Y, Wang C, Liu Z, et al. 3D printed conductive multiscale nerve guidance conduit with hierarchical fibers for peripheral nerve regeneration. *Adv Sci* 2023; 10(12): e2205744. DOI: 10.1002/advs.202205744.
82. Piola M, Soncini M, Cantini M, et al. Design and functional testing of a multichamber perfusion platform for three-dimensional scaffolds. *Sci World J* 2013; 2013: e123974. DOI: 10.1155/2013/123974.
83. Parrish J, Lim K, Zhang B, et al. New frontiers for biofabrication and bioreactor design in microphysiological system development. *Trends Biotechnol* 2019; 37(12): 1327–1343. DOI: 10.1016/j.tibtech.2019.04.009.
84. Wendt D, Marsano A, Jakob M, et al. Oscillating perfusion of cell suspensions through three-dimensional scaffolds enhances cell seeding efficiency and uniformity. *Biotechnol Bioeng* 2003; 84(2): 205–214. DOI: 10.1002/bit.10759.
85. Sun T, Norton D, Vickers N, et al. Development of a bioreactor for evaluating novel nerve conduits. *Biotechnol Bioeng* 2008; 99(5): 1250–1260. DOI: 10.1002/bit.21669.
86. Campbell N, Reece J, Urry L, et al. *Biologie*. 4e éd., volume 1. ERPI, 2012. ISBN 978-2-7613-2856-2.
87. Park D, Lee J, Chung JJ, et al. Integrating organs-on-chips: multiplexing, scaling, vascularization, and innervation. *Trends Biotechnol* 2020; 38(1): 99–112. DOI: 10.1016/j.tibtech.2019.06.006.
88. Ramamurthy P, White JB, Yull Park J, et al. Concomitant differentiation of a population of mouse embryonic stem cells into neuron-like cells and schwann cell-like cells in a slow-flow microfluidic device. *Dev DynOff Publ Am Assoc Anatom* 2017; 246(1): 7–27. DOI: 10.1002/dvdy.24466.
89. Sango K, Kawakami E, Yanagisawa H, et al. Myelination in coculture of established neuronal and Schwann cell lines. *Histochem Cell Biol* 2012; 137(6): 829–839. DOI: 10.1007/s00418-012-0934-3.
90. Gingras M, Beaulieu MM, Gagnon V, et al. In vitro study of axonal migration and myelination of motor neurons in a three-dimensional tissue-engineered model. *Glia* 2008; 56(3): 354–364. DOI: 10.1002/glia.20617.
91. Modrak M, Talukder MAH, Gurgenashvili K, et al. Peripheral nerve injury and myelination: potential therapeutic strategies. *J Neurosci Res* 2020; 98(5): 780–795. DOI: 10.1002/jnr.24538.